Peak Luminosity-Spectral Lag Relation Caused by the Viewing Angle of the Collimated Gamma-Ray Bursts

Kunihito Ioka[1] and Takashi Nakamura[2]

[1] Department of Physics, Kyoto University, Kyoto 606-8502, Japan

[2]Yukawa Institute for Theoretical Physics, Kyoto University, Kyoto 606-8502, Japan

Mar 2 2001

ABSTRACT

We compute the kinematical dependence of the peak luminosity, the pulse width and the spectral lag of the peak luminosity on the viewing angle θ_v of a jet. For appropriate model parameters we obtain the peak luminosity-spectral lag relation similar to the observed one including GRB980425. A bright (dim) peak with short (long) spectral lag corresponds to a jet with small (large) viewing angle. This suggests that the viewing angle of the jet might cause various relations in GRBs such as the peak luminosity-variability relation and the luminosity-width relation. Our model also suggests that X-ray rich GRBs (or X-ray flushes or Fast X-ray transients) are typical GRBs observed from large θ_v with large spectral lag and low variability.

Subject headings: gamma rays: bursts — gamma rays: theory

1. INTRODUCTION

Afterglows of the GRBs are believed to be produced by the external shocks while the GRB itself is by the internal shocks. There is a growing evidence that some of afterglows, such as GRB000926, GRB000301C, GRB990510 and GRB990123, are collimated with an opening half-angle of $\Delta\theta^{(a)} \sim 0.1$. However, the collimation half-angle $\Delta\theta$ of the internal shocks remains unknown since we can observe only the angular region inside the relativistic beaming half-angle $\sim \gamma^{-1}$ where γ is the Lorentz factor of the flow and is larger than ~ 100 to avoid the compactness problem (e.g., Piran 1999). Since the angular size of a causally connected region is also $\sim \gamma^{-1}$, the minimum possible $\Delta\theta$ is $\sim \gamma^{-1} \lesssim 10^{-2} \ll \Delta\theta^{(a)}$, that is, $\Delta\theta$ can be much smaller than $\Delta\theta^{(a)}$.

We here assume that the internal shocks consist of such sub-jets with the collimation half-angle of $\Delta\theta \ll \Delta\theta^{(a)}$. If we happen to observe a bright sub-jet, the isotropic luminosity

becomes very large so that the sub-jets model can interpret (1) no correlation between the gamma-ray fluence and the redshift, (2) the weak correlation between the gamma-ray fluence and the afterglow flux as well as (3) the extremely energetic bursts $\sim 10^{54}$ ergs (Kumar & Piran 2000; but see also Freedman & Waxman 1999). The X-ray pre/post-cursor (Murakami et al. 1991; Sazonov et al. 1998; in't Zand et al. 1999) can also be explained in the sub-jets model, if some of off-axis sub-jets are ejected earlier (for precursor) or later (for postcursor) than the main sub-jets (Nakamura 2000). X-ray rich GRBs (Strohmayer et al. 1998; Frontera et al. 2000; Heise et al. 2001; Kippen et al. 2001) are also expected in the sub-jets model if none of sub-jets point to our line-of-sight (Nakamura 2000). The "sub-jet" is sometimes termed "cannonball" (Dar & De Rújula 2000a, b; Plaga 2000), "mini-jet" (Shaviv & Dar 1995) and so on.

On the other hand, there are some possible relations between the peak luminosity, the spectral lag, the pulse width and the variability of GRBs. From six GRBs with known redshifts, Norris, Marani & Bonnell (2000) found that the isotropic peak luminosity is inversely proportional to the spectral lag which is defined as the time lag of the peak luminosity between different energy bands. Fenimore & Ramirez-Ruiz (2000) found that the luminosities of seven bursts with known redshifts are correlated with the variabilities of the bursts (see also Reichart et al. 2000). If both relations are correct, there should be a relation between the variability and the spectral lag. Recently Schaefer, Deng & Band (2001) showed that this is the case by plotting the variability and the spectral lag of 112 GRBs. Therefore at present there is a strong support that the luminosity-spectral lag as well as the luminosity-variability relation are correct.

There are several attempts to explain the luminosity-spectral lag and the luminosity-variability relations. Salmonson (2000, 2001) proposed that it is due to the difference of the observed cooling or deceleration time which depends on the variation in line-of-sight velocity among bursts. Schaefer (2001) interpreted the luminosity-spectral lag and luminosity-variability relation as a consequence of the conservation of energy when radiative cooling dominates and the dependence of the luminosity and variability on the Lorentz factor of the ejecta, respectively. However Wu & Fenimore (2000) pointed out that the synchrotron cooling time scale is much shorter than the lag time scale. Plaga (2000) argued that the luminosity-variability relation might be obtained in the framework of the cannonball model for the given power low power density spectrum of the GRBs.

In this Letter, under the assumption of short cooling time scale, we will show that depending on the viewing angle of a single jet to our line-of-sight, the luminosity-spectral lag and the luminosity-variability relation may arise kinematically. In the sub-jets model, we at present do not know the number of sub-jets in $\Delta\theta^{(a)}$. If it is small, that is, the filling

factor of the sub-jets is small, we should study effects of many independent sub-jets based on the present results of a single jet. If the number of sub-jets is large, we may apply the present results regarding $\Delta\theta \sim \Delta\theta^{(a)}$. In any case it is important to study the viewing angle dependence of various physical quantities, which is the main purpose of this Letter irrespective of the details of the sub-jets model.

2. INSTANTANEOUS EMISSION FROM AN EXPANDING THIN JET

The internal shock occurs in the relativistic wind when the fast moving flow catches up the slow one. The wind can be modeled by a succession of relativistic shells (Kobayashi, Piran & Sari 1997; Daigne & Mochkovitch 1998). A collision of two shells produces a single pulse light curve, whose superposition makes a whole light curve. Here we consider a single pulse. There are three time scales that determine the temporal pulse structure: the hydrodynamic time scale, the cooling time scale, and the angular spreading time scale (Kobayashi, Piran & Sari 1997; Katz 1997; Fenimore, Madras & Sergei 1996). The cooling time scale is usually much shorter than the hydrodynamic time scale in the internal shocks (Sari, Narayan & Piran 1996), so that we may assume a delta function time dependence of the emissivity in the comoving frame. Let l and L be the width of the shell and the separation of the shells. Then the hydrodynamic time scale $\sim l/c$ and the angular spreading time scale $\sim L/c$ determine the rise and the decay time of a single pulse, respectively. Since most observed pulses rise more quickly than they decay (Norris et al. 1996), for simplicity we may adopt an infinitesimally thin shell approximation as $l \ll L$.

Let us consider an emitting thin shell that is confined to a cone of an opening half-angle $\Delta\theta$ and moves radially outward with the Lorentz factor of $\gamma = 1/\sqrt{1-\beta^2}$. A general formula to calculate the observed flux from an optically thin material is derived by Granot, Piran & Sari (1999) and Woods & Loeb (1999). Here we adopt their formulations and notations. Let us use a spherical coordinate system $\boldsymbol{r} = (r, \theta, \phi)$ in the lab-frame, where the $\theta = 0$ axis points toward the detector and the central engine is located at the origin. Let also the detector be at a distance D from the source and $\alpha := r\sin\theta/D = r\sqrt{1-\mu^2}/D$ be the angle that a given ray makes with the $\theta = 0$ axis. Then the observed flux at the observed time T, measured in erg s^{-1} cm^{-2} Hz^{-1}, is given by $F_\nu(T) = \frac{\nu D}{\gamma\beta} \int_0^{2\pi} d\phi \int_0^{\alpha_m} \alpha^2 d\alpha \int_{\nu\gamma(1-\beta)}^{\nu\gamma(1+\beta)} \frac{d\nu'}{\nu'^2} \frac{j'_{\nu'}(\Omega'_d, \boldsymbol{r}, t)}{(1-\mu^2)^{3/2}}$ and $\mu = (1 - \nu'/\gamma\nu)/\beta$, where Ω'_d, $t = T + (r\mu/c)$, α_m, and $j'_{\nu'}$ are the direction towards the detector measured in the comoving frame, the lab-frame time, the maximum value of α, and the comoving frame emissivity in units of ergs s^{-1} cm^{-3} Hz^{-1} sr^{-1}. Note here that a prime means the physical quantities in the comoving frame.

If the emission is isotropic in the comoving frame, the emissivity has a functional form

of $j'_{\nu'}(\Omega'_d, \boldsymbol{r}, t) = A_0 f(\nu')\delta(t - t_0)\delta(r - r_0)H(\Delta\theta - |\theta - \theta_v|)H\left[\cos\phi - \left(\frac{\cos\Delta\theta - \cos\theta_v\cos\theta}{\sin\theta_v\sin\theta}\right)\right]$,
where $f(\nu')$ represents the spectral shape and θ_v is the angle that the axis of the emission cone makes with the $\theta = 0$ axis. The delta functions describe an instantaneous emission at $t = t_0$ and $r = r_0$, and $H(x)$ is the Heaviside step function which describes that the emission is inside the cone. Then, the flux of a single pulse is given by

$$F_\nu(T) = \frac{2cA_0 r_0 \gamma^2}{D^2}\frac{\Delta\phi(T)f\left[\nu\gamma(1 - \beta\cos\theta(T))\right]}{\left[\gamma^2(1 - \beta\cos\theta(T))\right]^2}, \tag{1}$$

where $1 - \beta\cos\theta(T) = (c\beta/r_0)(T - T_0)$ and $T_0 = t_0 - r_0/c\beta$. For $\Delta\theta > \theta_v$ and $0 < \theta(T) \leq \Delta\theta - \theta_v$, $\Delta\phi(T) = \pi$, otherwise $\Delta\phi(T) = \cos^{-1}\left[\frac{\cos\Delta\theta - \cos\theta(T)\cos\theta_v}{\sin\theta_v\sin\theta(T)}\right]$. For $\theta_v < \Delta\theta$, $\theta(T)$ varies from 0 to $\theta_v + \Delta\theta$ while from $\theta_v - \Delta\theta$ to $\theta_v + \Delta\theta$ for $\theta_v > \Delta\theta$. In the latter case, $\Delta\phi(T) = 0$ for $\theta(T) = \theta_v - \Delta\theta$.

The observed spectrum of GRBs is well approximated by the Band spectrum (Band et al. 1993). In order to have a spectral shape similar to the Band spectrum, we adopt the following form of the spectrum in the comoving frame,

$$f(\nu') = \left(\frac{\nu'}{\nu'_0}\right)^{1 + \alpha_B}\left[1 + \left(\frac{\nu'}{\nu'_0}\right)^s\right]^{(\beta_B - \alpha_B)/s}, \tag{2}$$

where α_B (β_B) is the low (high) energy power law index, and s describes the smoothness of the transition between the high and low energy. $\alpha_B \sim -1$ and $\beta_B \sim -2.5$ are typical values (Preece et al. 2000). Equations (1) and (2) are the basic equations to calculate the flux of a single pulse, which depends on nine parameters for $\theta_v \ll 1$ and $\Delta\theta \ll 1$: $\gamma\nu'_0$, $\gamma\theta_v$, $\gamma\Delta\theta$, $r_0/c\beta\gamma^2$, $T_0 = t_0 - r_0/c\beta$, α_B, β_B, s and $2cA_0 r_0\gamma^2/D^2$.

3. PULSE PROFILE AND SPECTRUM

In order to study the viewing angle dependence of a pulse from a single jet, we first fix other parameters: $\gamma\Delta\theta = 1$, $\alpha_B = -1$, $\beta_B = -2.5$ and $s = 1$. The lab-frame frequency, the observed time and the flux per frequency are measured in units of $\gamma\nu'_0$, $r_0/c\beta\gamma^2$ and $2cA_0 r_0\gamma^2/D^2$, respectively. The total fluence is given by $S_\nu = \int_{T_{start}}^{T_{end}} F_\nu(T)dT$, where $T_{start} = T_0 + (r_0/c\beta)(1 - \beta\cos(\max[0, \theta_v - \Delta\theta]))$ and $T_{end} = T_0 + (r_0/c\beta)(1 - \beta\cos(\theta_v + \Delta\theta))$. In Figure 1, we plot νS_ν as a function of the observed frequency ν by varying the viewing angle $\gamma\theta_v$. As $\gamma\theta_v$ increases, both the maximum frequency and νS_ν decrease. Here the maximum frequency ν_{max} means the frequency at which most of the radiation energy is emitted. In Figure 1 we also show the analytically estimated dependence, $\nu_{max} \propto \delta^{-1}$ and $(\nu S_\nu)_{max} \propto \delta^{-3}$, by triangles, where $\delta = \gamma(1 - \beta\cos\theta_v) \simeq (1 + \theta_v^2\gamma^2)/2\gamma$ is the Doppler

factor (see Ioka & Nakamura 2001 for analytical estimates.). Figure 1 shows that if we observe the jet from $\theta_v \sim$ several $\times \gamma^{-1}$ the maximum frequency ν_{max} is in the X-ray band while for $\theta_v \sim \gamma^{-1}$ it is in the gamma-ray region so that depending on the viewing angle, GRBs may be observed as X-ray rich GRBs in our model (Nakamura 2000). Note that if the emitting sub-jets distribute sparsely within the opening angle of the afterglow $\Delta\theta^{(a)}$ or if we are seeing the edge of the afterglow cone, the afterglow can occur as usual.

Several pulse profiles are shown in the upper panel of Figure 2, where the observed frequency is taken as $\nu = 200\text{keV}(\gamma\nu'_0/10^3\text{keV})$. The pulse profiles are similar to the FRED (Fast Rise Exponential Decay) shape observed in many bursts. Note here that the vertical axis is a log scale so that the straight line means the exponential decay. In the lower panels of Figure 2 we show the pulse width W_{FWHM} at half maximum and the product of the peak flux and the width $\nu F_\nu^{peak} W_{FWHM}$ as a function of $(1 + \gamma^2\theta_v^2) \propto \delta$ with the analytically estimated dependence on $(1 + \gamma^2\theta_v^2)$ (see Ioka & Nakamura 2001). Figure 2 shows that the luminosity-width relation is given by $\nu F_\nu^{peak} \propto W_{FHWM}^\kappa$ where $\kappa = -2 + \alpha_B \sim -3$ for $\theta_v \sim \Delta\theta$ and $\gamma\theta_v \lesssim [10(\gamma\nu'_0/10^3\text{keV})(\nu_{obs}/200\text{keV})^{-1} - 1]^{1/2}$. This is consistent with the observation that the narrower pulse tends to be brighter in each burst following $\nu F_\nu^{peak} \propto W_{FWHM}^{-2.8}$ (Ramirez-Ruiz & Fenimore 2000). Our calculations predict that the exponent κ ranges from $\kappa = -2 + \alpha_B \sim -3$ to $\kappa = -3 + 2\beta_B \sim -8$ for dimmer bursts including X-ray rich GRBs which have the larger viewing angle in our model.

4.   PEAK LUMINOSITY-SPECTRAL LAG/VARIABILITY RELATION

In the upper panel of Figure 3, varying the viewing angle $\gamma\theta_v$ we show the isotropic peak luminosity at frequency $\nu_\gamma = 200\text{keV}(\gamma\nu'_0/10^3\text{keV})$ as a function of the spectral lag in an arbitrary vertical scale of $2cA_0 r_0\gamma^2/D^2$. For simplicity, we define the spectral lag ΔT as the difference of the peak time between frequencies $\nu_\gamma = 200\text{keV}(\gamma\nu'_0/10^3\text{keV})$ and $\nu_X = 20\text{keV}(\gamma\nu'_0/10^3\text{keV})$, although the spectral lag is determined by the cross-correlation analysis in Norris, Marani & Bonnell (2000). Since there is no lag when the observer is inside the emission cone $\theta_v < \Delta\theta$ in our present definition, all points with $\Delta T \leq 10^{-4}(r_0/c\beta\gamma^2)$ are plotted at $\Delta T = 10^{-4}(r_0/c\beta\gamma^2)$. In the lower panel of Figure 3 the solid line shows the corresponding viewing angle $\gamma\theta_v$ as a function of ΔT. We adopt $r_0/c\beta\gamma^2 = 10$ s. The peak luminosity first decreases with increasing spectral lag and turns back for large spectral lag since the different θ_v give the same lag. The analytical estimates, $\nu F_\nu^{peak} \propto \Delta T^{-3/2}$ and $\gamma\theta_v \propto \Delta T^{1/4}$, shown by dotted lines agree well with the solid lines for $1 \lesssim \gamma\theta_v \lesssim 3$ (see Ioka & Nakamura 2001). The deviation from the power law at low luminosity is due to the fact that the maximum frequency ν_{max} becomes lower than the observed gamma-ray

frequency ν_γ (see Figure 1). The observed luminosity-spectral lag relations for seven bursts with known redshifts (Norris, Marani & Bonnell 2000) are also plotted for comparison. Surprisingly enough, a simple sub-jet model happens to reproduce the observation quite well including GRB980425 which has the extremely dim luminosity and large spectral lag.

The sub-jets model might be compatible with the luminosity-variability relation that more complex bursts tend to be brighter (Fenimore & Ramirez-Ruiz 2000; Reichart et al. 2000; Schaefer, Deng & Band 2001). According to Plaga (2000), when the power density spectrum of the GRB time histories is $P \propto f^d \sim f^{-5/3}$ (Beloborodov, Stern & Svensson 1998, 2000; Shaviv & Dar 1995), the variability relates to the pulse width as $V \propto \delta^{d+1} \propto W_{FHWM}^{d+1}$. From Figure 2 and §3, the peak flux at a given frequency depends on the pulse width as $\nu F_\nu^{peak} \propto W_{FHWM}^\kappa$. Therefore the luminosity-variability relation is given by $\nu L_\nu^{peak} \propto V^{\kappa/(d+1)} \sim V^{4.5}(V^{12})$ for the brightest (dimmest) bursts. In the upper panel of Figure 4, we show $\nu L_\nu^{peak} \propto V^{\kappa/(d+1)}$ by the solid line , using νL_ν^{peak} and W_{FHWM} in Figure 2 and §3 with appropriate off-sets. The observed luminosity-variability relations for eight bursts with known redshifts (Fenimore & Ramirez-Ruiz 2000) are also plotted for comparison. Surprisingly again, a simple sub-jet model happens to reproduce the observation quite well including GRB980425 which has the extremely low variability. Although the power density spectrum of the GRBs has been assumed, this agreement together with the results of the luminosity-spectral lag relation suggests that a single sub-jet model may capture the main features of the GRBs.

5.   DISCUSSIONS

GRB980425 and its apparent association with SN1998bw first provided a possible connection between GRBs and SNe. Since GRB980425 was an unusual GRB, it may be a new type of GRB. However, we have shown that the unusually low luminosity, large spectral lag and low variability of GRB980425 can be interpreted by the off-axis sub-jet emission with the viewing angle of $\theta_v \sim 10/\gamma \sim 6°$. The off-axis sub-jet emission may also explain why GRB980425 was not seen in BATSE's highest energy band (> 300keV; Norris, Marani & Bonnell 2000), since the maximum frequency ν_{max} becomes lower than the observed frequency from Figure 1. Furthermore, the unusually slowly declining X-ray afterglow of GRB980425 ($\propto T^{-0.2}$) can also be explained by the off-axis emission from the collimated afterglow with the viewing angle of $\theta_v^{(a)} \sim 30°$ (Nakamura 1999). Since the axis of the afterglow can differ from that of the sub-jet, $\theta_v \sim 6°$ is compatible with $\theta_v^{(a)} \sim 30°$ if the sub-jets on the edge of the afterglow were seen. Moreover from the late time light curve of SN1998bw, it is suggested that the explosion is jet-like and our line-of-sight is off-axis

from the jet (Maeda et al. 2000). Therefore GRB980425 may be a typical GRB observed from the large viewing angle so that our results have strengthened the association of GRBs with SNe.

The bright bursts, such as GRB990123, can be suspected of on-axis emission with no or little spectral lag in our model, so that observation with fine time resolution is important to measure very small lag. In reality, a burst should have more or less off-axis emission so that the lag should exist in the cross-correlation analysis (Norris, Marani & Bonnell 2000; Wu & Fenimore 2000). In this Letter we have studied only the behavior of the single sub-jet under the simple treatment of the spectral lag. Nevertheless we have obtained theoretical results very similar to the observations, which suggests the viewing angle is one of the most important factors to determine the various relations in GRBs. In the next step we should consider the multiple sub-jets case using the present results of the single sub-jet.[1]

REFERENCES

Band, D., et al. 1993, ApJ, 413, 281

Beloborodov, A. M., Stern, B. E., & Svensson, R. 1998, ApJ, 508, L25

Beloborodov, A. M., Stern, B. E., & Svensson, R. 2000, ApJ, 535, 158

Daigne, F., & Mochkovitch, R. 1998, MNRAS, 296, 275

Dar, A., & De Rújula, A. 2000a, astro-ph/0008474

Dar, A., & De Rújula, A. 2000b, astro-ph/0012227

Fenimore, E. E., Madras, C. D., & Sergei, N. 1996, ApJ, 473, 998

Fenimore, E., & Ramirez-Ruiz, E. 2000, astro-ph/0004176

Frail, D. A., et al. 2001, astro-ph/0102282

---

[1]When we almost completed this Letter, Frail et al. (2001) suggested that GRBs with the narrower $\Delta\theta^{(a)}$ tend to have larger isotropic gamma-ray total energy. In our model this suggests that the filling factor of the sub-jets within $\Delta\theta^{(a)}$ is another key parameter.

Freedman, D. L., & Waxman, E. 1999, astro-ph/9912214

Frontera, F., et al. 2000, ApJ, 540, 697

Granot, J., Piran, T., & Sari, R. 1999, ApJ, 513, 679

Heise, J., et al. 2001, in Proc. Second Rome Workshop: Gamma-Ray Bursts in the Afterglow Era

in't Zand, J. J. M., Heise, J., van Paradijs, J., & Fenimore, E. E. 1999, ApJ, 516, L57

Ioka, K., & Nakamura, T. 2001, in preparation

Katz, J. I. 1997, ApJ, 490, 633

Kippen, R. M., et al. 2001, in Proc. Second Rome Workshop: Gamma-Ray Bursts in the Afterglow Era, astro-ph/0102277

Kobayashi, S., Piran, T., & Sari, R. 1997, ApJ, 490, 92

Kumar, P., & Piran, T. 2000, ApJ, 535, 152

Maeda, K., et al. 2000, astro-ph/0011003

Murakami, T., et al. 1991, Nature, 350, 592

Nakamura, T. 1999, ApJ, 522, L101

Nakamura, T. 2000, ApJ, 534, L159

Norris, J. P., et al. 1996, ApJ, 459, 393

Norris, J. P., Marani, G. F., & Bonnell, J. T. 2000, ApJ, 534, 248

Piran, T. 1999, Phys. Rep., 314, 575

Plaga, R. 2000, astro-ph/0012060

Preece, R. D., et al. 2000, ApJS, 126, 19

Ramirez-Ruiz, E., & Fenimore, E. E. 2000, ApJ, 539, 712

Reichart, D. E., et al. 2000, astro-ph/0004302

Rybicki, G. B., & Lightman, A. P. 1979, Radiative Processes in Astrophysics (New York: Wiley Interscience)

Salmonson, J. D. 2000, ApJ, 544, L115

Salmonson, J. D. 2001, ApJ, 546, L29

Sazonov, S. Y., et al. 1998, A&AS, 129, 1

Schaefer, B. E. 2001, astro-ph/0101462

Schaefer, B. E., Deng, M., & Band, D. L. 2001, astro-ph/0101461

Shaviv, N. J., & Dar, A. 1995, ApJ, 447, 863

Sari, R., Narayan, R., & Piran, T. 1996, ApJ, 473, 204

Strohmayer, T. E., et al. 1998, ApJ, 500, 873

Woods, E., & Loeb, A. 1999, ApJ, 523, 187
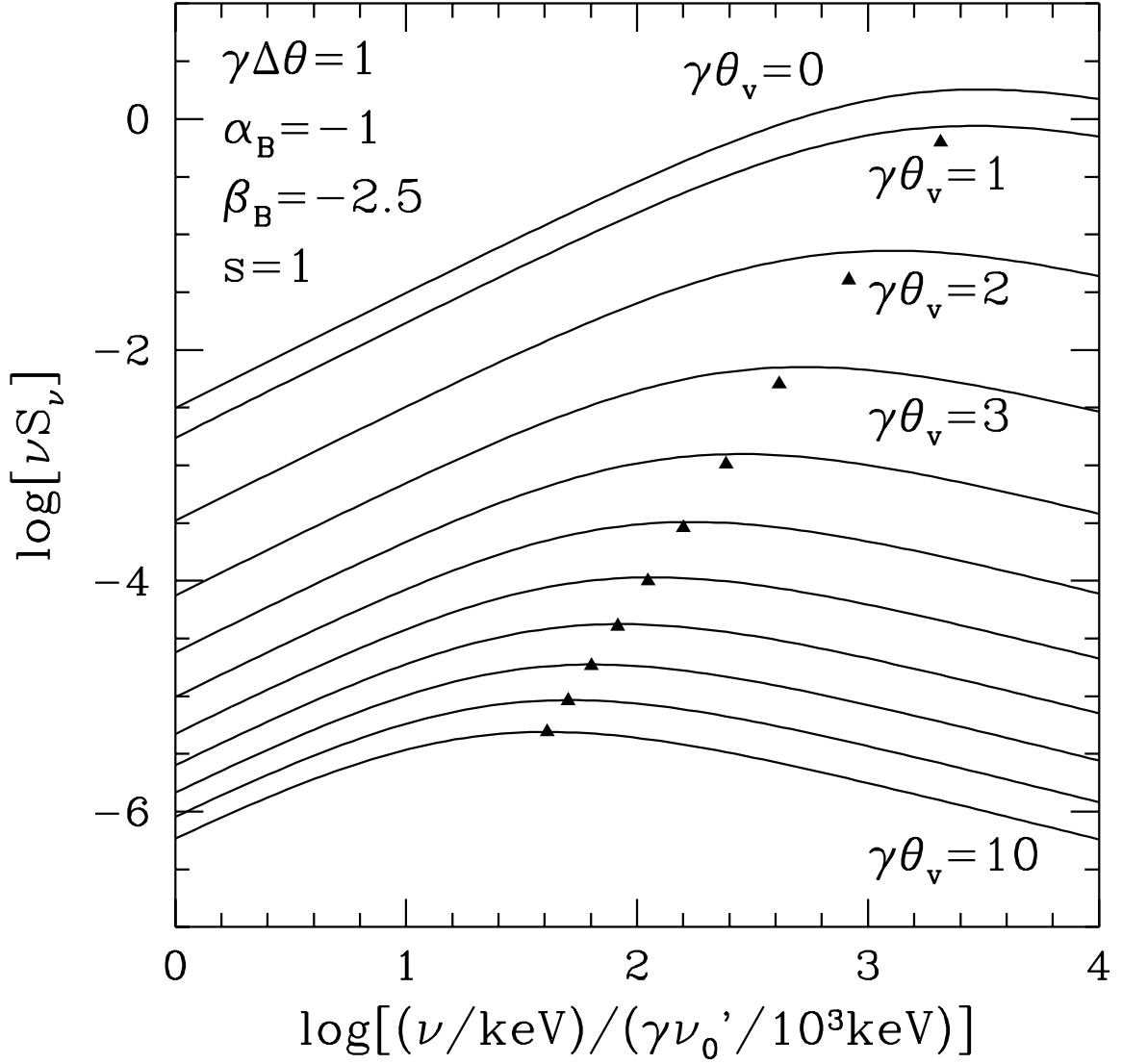
Wu, B., & Fenimore, E. 2000, ApJ, 535, L29

Fig. 1.— The total fluence νS_ν in units of $2A_0 r_0^2 \gamma \nu_0'/\beta D^2$ is shown as a function of the observed frequency by varying the viewing angle $0 \leq \gamma\theta_v \leq 10$, ($\gamma\theta_v$: integer). We adopt $\gamma\Delta\theta = 1$, $\alpha_B = -1$, $\beta_B = -2.5$ and $s = 1$. The triangles represent the analytically estimated dependence, $\nu_{max} \propto \delta^{-1}$ and $(\nu S_\nu)_{max} \propto \delta^{-3}$, where $\delta = \gamma(1 - \beta\cos\theta_v) \simeq (1 + \theta_v^2\gamma^2)/2\gamma$ is the Doppler factor and the normalization is set by the peak of $\gamma\theta_v = 10$.
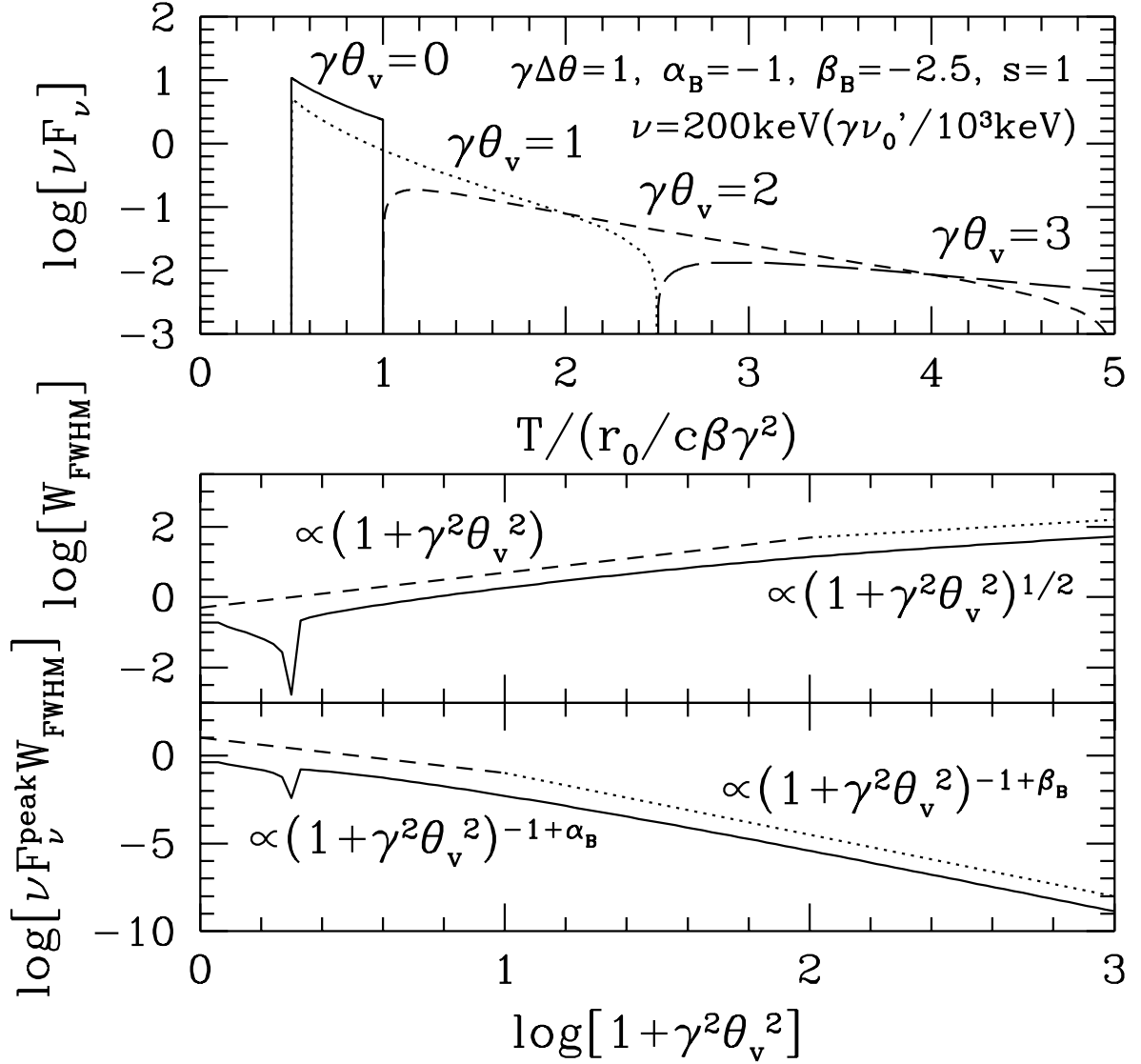
Fig. 2.— (*upper panel*): Pulse profiles are shown. The pulse begins at $T_{start} = T_0 + (r_0/c\beta)(1 - \beta\cos(\max[0, \theta_v - \Delta\theta]))$ and ends at $T_{end} = T_0 + (r_0/c\beta)(1 - \beta\cos(\theta_v + \Delta\theta))$. Here we set $T_0 = 0$. (*middle panel*): The pulse width W_{FWHM} at half maximum in units of $r_0/c\beta\gamma^2$ is shown as a function of $(1 + \gamma^2\theta_v^2)$. The pulse width W_{FWHM} can be estimated as $W_{FWHM} \propto \delta \propto (1+\gamma^2\theta_v^2)$ for $\theta_v \sim \Delta\theta$ and $W_{FWHM} \propto \delta^{1/2} \propto (1+\gamma^2\theta_v^2)^{1/2} \sim \gamma\theta_v$ for $\theta_v \gg \Delta\theta$, which are shown by dashed and dotted lines, respectively. (*lower panel*): The product of the peak flux νF_ν^{peak} and the pulse width W_{FWHM}, in units of $2A_0r_0^2\gamma\nu_0'/\beta D^2$, is shown as a function of $(1+\gamma^2\theta_v^2)$. This quantity is about the total fluence νS_ν in Figure 1. The peak flux νF_ν^{peak} can be estimated from the relation $\nu F_\nu^{peak}W_{FWHM} \sim \nu S_\nu \propto \delta^{-1+\alpha_B}(\delta^{-1+\beta_B})$ when the maximum frequency ν_{max} is higher (lower) than the observed frequency, which are shown by dashed (dotted) lines. In all panels, we adopt $\gamma\Delta\theta = 1$, $\alpha_B = -1$, $\beta_B = -2.5$ and $s = 1$, and the observed frequency is $\nu = 200\text{keV}(\gamma\nu_0'/10^3\text{keV})$.
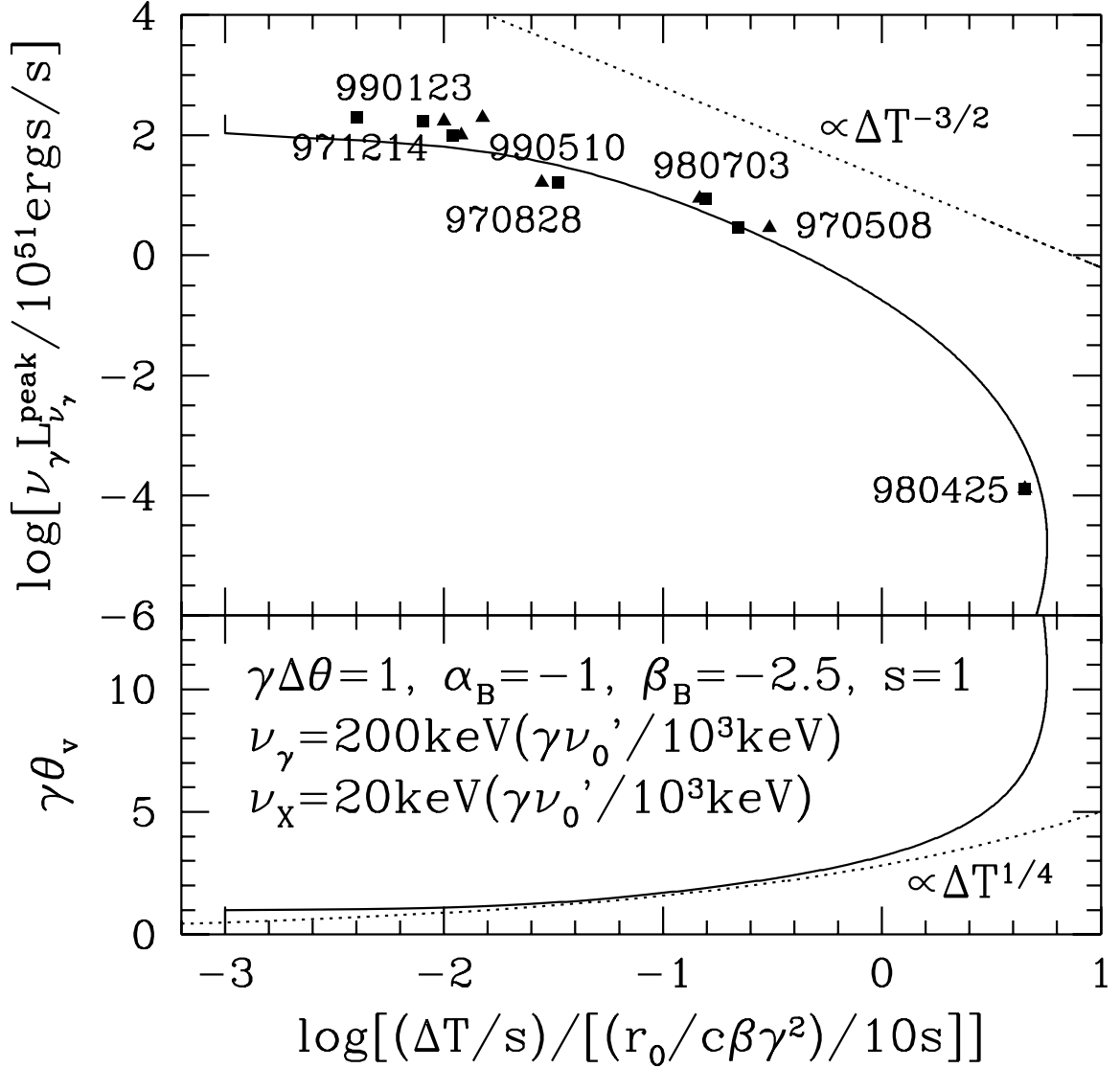
Fig. 3.— The isotropic peak luminosity at frequency $\nu_\gamma = 200\text{keV}(\gamma\nu_0'/10^3\text{keV})$ is shown as a function of the spectral lag of the peak time ΔT by varying the viewing angle $\gamma\theta_v$. The corresponding viewing angle $\gamma\theta_v$ is shown in the lower panel. The spectral lag ΔT is defined by the difference of the peak time between frequencies $\nu_\gamma = 200\text{keV}(\gamma\nu_0'/10^3\text{keV})$ and $\nu_X = 20\text{keV}(\gamma\nu_0'/10^3\text{keV})$. We adopt $\gamma\Delta\theta = 1$, $\alpha_B = -1$, $\beta_B = -2.5$, $s = 1$, $r_0/c\beta\gamma^2 = 10$ s and an arbitrary vertical unit $2cA_0r_0\gamma^2/D^2$. All points with $\Delta T \leq 10^{-4}(r_0/c\beta\gamma^2)$ are plotted at $\Delta T = 10^{-4}(r_0/c\beta\gamma^2)$. The observed luminosity-spectral lag relations for seven bursts with known redshifts are shown from Table 1 in Norris, Marani & Bonnell (2000). Squares and triangles are lags for regions down to 0.5 and 0.1 of the peak luminosity, respectively. The dotted lines represent the power law behavior $\nu_\gamma L_{\nu_\gamma}^{peak} \propto \Delta T^{(-2+\alpha_B)/(s+1)} = \Delta T^{-3/2}$ and $\gamma\theta_v \propto \Delta T^{1/2(s+1)} = \Delta T^{1/4}$ (Ioka & Nakamura 2001).
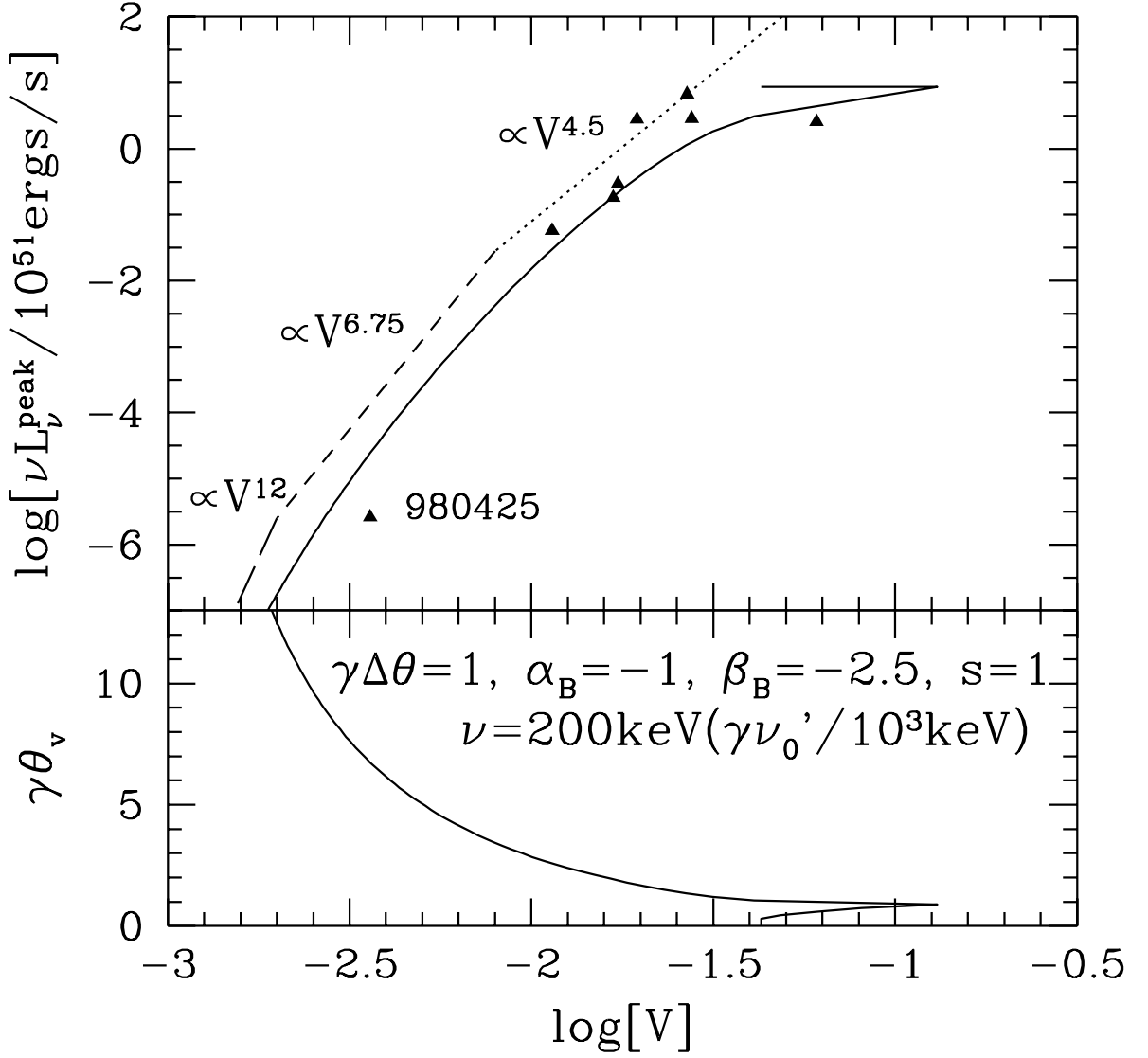
Fig. 4.— The isotropic peak luminosity at frequency $\nu = 200\text{keV}(\gamma\nu_0'/10^3\text{keV})$ is shown as a function of the variability V by varying the viewing angle $\gamma\theta_v$. The corresponding viewing angle $\gamma\theta_v$ is shown in the lower panel. We adopt $\gamma\Delta\theta = 1$, $\alpha_B = -1$, $\beta_B = -2.5$, $s = 1$, the power density spectrum of the GRB time histories $P \propto f^d \sim f^{-5/3}$, and appropriate offsets. The observed luminosity-variability relations for seven bursts with known redshifts are shown by filled triangles from Table 1 of Fenimore & Ramirez-Ruiz (2000). The analytical estimates of $\nu L_\nu^{peak} \propto V^{(-2+\alpha_B)/(d+1)} \sim V^{4.5}$, $\nu L_\nu^{peak} \propto V^{(-2+\beta_B)/(d+1)} \sim V^{6.75}$, and $\nu L_\nu^{peak} \propto V^{(-3+2\beta_B)/(d+1)} \sim V^{12}$ are shown in each region by dotted, dashed, and long dashed lines, respectively.